

© 2023 Society of Photo-Optical Instrumentation Engineers (SPIE)

Citation: N. C. Gellert, K. K. Madsen, S. Massahi, D. Sanz, D. D. M. Ferreira, S. Svendsen, A. S. Jegers, and F. E. Christensen "Investigation of NiV-based multilayers for the high energy x-ray probe", Proc. SPIE 12679, Optics for EUV, X-Ray, and Gamma-Ray Astronomy XI, 126791F (5 October 2023); <https://doi.org/10.1117/12.2676128>

DOI: <https://doi.org/10.1117/12.2676128>

Access to this work was provided by the University of Maryland, Baltimore County (UMBC) ScholarWorks@UMBC digital repository on the Maryland Shared Open Access (MD-SOAR) platform.

Please provide feedback

Please support the ScholarWorks@UMBC repository by emailing scholarworks-group@umbc.edu and telling us what having access to this work means to you and why it's important to you. Thank you.

PROCEEDINGS OF SPIE

[SPIDigitalLibrary.org/conference-proceedings-of-spie](https://spiedigitallibrary.org/conference-proceedings-of-spie)

Investigation of NiV-based multilayers for the high energy x-ray probe

N. C. Gellert, K. Madsen, S. Massahi, D. Sanz, D. D. M. Ferreira, et al.

N. C. Gellert, K. K. Madsen, S. Massahi, D. Sanz, D. D. M. Ferreira, S. Svendsen, A. S. Jegers, F. E. Christensen, "Investigation of NiV-based multilayers for the high energy x-ray probe," Proc. SPIE 12679, Optics for EUV, X-Ray, and Gamma-Ray Astronomy XI, 126791F (5 October 2023); doi: 10.1117/12.2676128

SPIE.

Event: SPIE Optical Engineering + Applications, 2023, San Diego, California, United States

Investigation of NiV-based multilayers for the High Energy X-ray Probe

N. C. Gellert^a, K. K. Madsen^{b,c}, S. Massahi^a, D. Sanz^a, D. D. M. Ferreira^a, S. Svendsen^a, A. 'S Jegers^a, and F. E. Christensen^a

^aDTU Space, Technical University of Denmark, Elektrovej 328, 2800, Kgs. Lyngby, Denmark

^bCRESST and X-ray Astrophysics Laboratory, NASA Goddard Space Flight Center, Greenbelt, MD 20771, USA

^cDepartment of Physics and Center for Space Science and Technology, University of Maryland, Baltimore County, Baltimore, MD 21250, USA

ABSTRACT

The High Energy X-ray Probe (HEX-P) is a NASA probe-class mission concept that will combine high spatial resolution X-ray imaging (<10 arcsec FWHM) and broad spectral coverage (0.1–150 keV) with an effective area far superior to current facilities (including XMM-Newton and NuSTAR) to enable revolutionary new insights into a variety of important astrophysical problems. Optimized nanometer-thin Ni-based multilayer coatings enable high performance of focusing X-ray telescopes to energies up to 150 keV and beyond, though current fabricated Ni-based coatings contain high interfacial roughness which will affect the predicted performance of the telescope. As part of the thin film coating development for the High Energy X-ray Probe, we report on the current development of reducing the coating roughness in periodic NiV/Si multilayer coatings. The multilayers are fabricated using the direct current magnetron sputtering coating facility at DTU Space, using different types of sputtering collimators and different reactive sputtering gas concentrations, optimized for the production of low interfacial roughness. The multilayers are characterized using X-ray reflectometry and X-ray photoelectron spectroscopy. More information on HEX-P, including the full team list, is available at hexp.org.

Keywords: Thin film coating, HEX-P, Multilayer, Focusing X-ray optics, Reactive sputtering, DC magnetron sputtering, Collimation, X-ray reflectometry.

1. INTRODUCTION

With the loss of the Japan Aerospace Exploration Agency (JAXA) Hitomi X-ray observatory,^{1,2} the American Nuclear Spectroscopic Telescope Array (NuSTAR^{3–5}) is currently the only operating high-energy (> 30 keV) focusing X-ray telescope with direct-imaging which has greatly exceeded the expected mission duration. NuSTAR and Hitomi utilize grazing incidence X-ray reflection where the effective energy bandwidths are limited by the absorption edges of their reflector material platinum (Pt).

The High Energy X-ray Probe (HEX-P) is the next-generation general purpose X-ray observatory, designed by the National Aeronautics and Space Administration (NASA). HEX-P will have two High Energy Telescopes (HET) which will have an unprecedented broad bandpass from 2 to 150 keV, and be able to resolve the cosmic history of the X-ray background at its peak with more accuracy than NuSTAR and Chandra⁶. HEX-P will provide an unprecedented opportunity to probe the accretion physics from black holes and neutron stars, reveal detailed studies of the circum-nuclear environment surrounding active galactic nuclei that will shed light on the intrinsic nature of merging supermassive black holes, and constrain the endpoints of stellar evolution and compact object mergers⁷. HEX-P will use a much longer focal length at 20 m, making use of total external reflection to extend the band pass to significantly higher energy than NuSTAR and Hitomi. The material selection for HEX-P is not yet determined, though platinum (Pt) and nickel (Ni) are the favorite candidates for the reflecting

Further author information:

Nis. C. Gellert: e-mail: nige@space.dtu.dk, telephone: (+45) 45 25 97 45

Optics for EUV, X-Ray, and Gamma-Ray Astronomy XI, edited by Stephen L. O'Dell,
Jessica A. Gaskin, Giovanni Pareschi, Daniele Spiga, Proc. of SPIE Vol. 12679,
126791F · © 2023 SPIE · 0277-786X · doi: 10.1117/12.2676128

material. Pt is flown on both NuSTAR and Hitomi, and its thin film properties are well known. However, Ni has the K-absorption edge at 8.3 keV and therefore does not have the same restriction as Pt, making it possible to achieve the required broadband. Beyond the critical (cut-off) energy, the reflectance can be enhanced by using nanometer-thin multilayer coatings which act as lattice spacing in a crystal separated by the distance d . However, Ni thin films are known to exhibit a high surface and interfacial roughness, and therefore it is important to evaluate if Ni-based multilayers can be produced to meet the roughness requirement, in order to assure high performance and long-term stability.

The surface and interfacial roughness of thin films depend on the target material properties, but also on the substrate (mirror) conditions, and on deposition methods and capabilities. In this work, a nickel vanadium (Ni_{93}V_7) and silicon (Si) sputtering target is used to sputter NiV/Si multilayers with a periodic 10 bilayer structure. This paper reports on the current status of developing NiV/Si multilayers for HEX-P. We present different types of sputtering collimators and different reactive sputtering gas concentrations using molecular nitrogen (N_2) and argon (Ar). The multilayers are characterized using 8.048 keV X-ray reflectometry (XRR) and X-ray photoelectron spectroscopy (XPS). Lastly we have evaluated the thin film contamination due scattering of sputtering atoms in the coating chamber. In previous studies at DTU Space, visual remnants of sputtering have been observed in areas outside the theoretical field of view of the sputtered atoms.

2. COATING CONSIDERATIONS

Studies using native Ni and Ni compound targets show that the deposited Ni thin films tend to have or induce high interfacial roughness⁸⁻¹². In order for HEX-P to have flight optics modules with thin film coatings consisting of Ni, the roughness has to be drastically lowered compared to the current production state. There are multiple factors that affect the residual interfacial roughness in the thin film that are dependant on the material target, such as the grain size, crystal orientation, magnetic properties, residual stresses etc.⁸⁻¹⁰ Multiple process conditions¹³ can effect the thin film, such as the substrate temperature, substrate bias voltage, growth rate, barrier layers at the interfaces,¹⁴ sputtering gas,¹² pressure,¹⁵ incidence of the sputtered material,¹⁶⁻¹⁸ collimation,¹² contamination etc. Finally, the different deposition methods such as physical and plasma vapor deposition, sputtering and chemical vapor deposition etc.

In this work, DC magnetron sputtering is used due to being suited for mass production, though other deposition methods can produce Ni thin film with a lower roughness¹⁵ and a finer grain size, than the films obtained by using DC magnetron sputtering¹⁰. We use a nickel vanadium (Ni_{93}V_7) sputtering target, since the small amount of vanadium makes the target non-magnetic, ensuring uninterrupted electric and magnetic field lines from the magnetron.¹⁹ The material we used in this work that acts a spacer in the multilayer structure, is a silicon (Si) target. An image of the Si and NiV targets are shown in Figure 1 where it is observed that the NiV target has a considerably larger visual surface roughness, relative to the Si target. Though this is not directly related to the magnitude of the sputtered roughness.

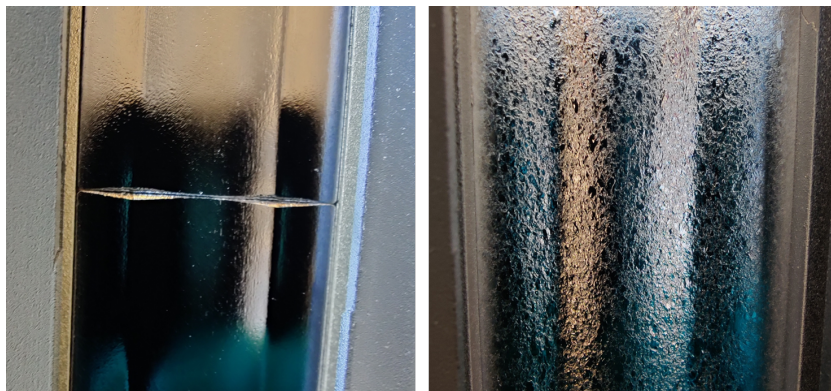


Figure 1: Close-up image of the Si target (left) and NiV target (right) used in this paper.

It has been shown that the collimation of the sputtered particles plays an important role in the production of thin film coatings with low roughness.^{16,17} Collimation reduces the solid angle of the sputtered particles and reduces the angles of incidence of the sputtered material onto the mirror. In this work, we evaluate the separator plate (SP) collimation and honey-comb (HC) collimation presented by A. Vickery et. al.,¹⁷ and shown in Figure 2 and Figure 3. We also evaluated a new target collimator (TC) that is shown in Figure 3 which will reduce the maximum horizontal incidence angle of the sputtered material reaching the sample.

The standard design of the magnetron includes the side-ears (SE) illustrated in Figure 3 which are electrically floating stainless steel shields, and provide a horizontal collimation which prevent the material sputtered with an angle above $\theta_{SE} = 63.7^\circ$. The SE are used in all coatings presented in this work.

The separator plate (SP) collimation is developed for curved substrates used on NuSTAR,¹⁷ as illustrated in Figure 2, and the current HEX-P optics design includes curved mirrors. The SP provide a vertical collimation of the sputtered particles reaching the mirror, with an an opening angle where the maximum incidence angle of the sputtered material reaching the sample is $\theta_{SP} = 47.7^\circ$. The SP are used in all coatings presented in this work.

The zirconium oxide (ZrO_x) coated aluminium (Al) honey-comb (HC) collimation is mounted on the SE shielding, and therefore it is also electrically floating. The HC is shown and illustrated in Figure 3, providing a horizontal and vertical collimation. The mesh is mounted at a 42 mm distance from the target surface, so no sputtering of the honeycomb occurs. The XPS results presented in this paper showed no evidence of Zr and Al. The mesh thickness is 5 mm with a cell diameter of 6.4 mm which provides a solid angle of $\theta_{HC} = 52.7^\circ$, hence there is no patterning of the substrate from the mesh.¹⁷

The target collimator (TC) is mounted as an extension of the SE collimation and therefore also electrically floating, as presented in figure 3. The TC is angled at a 45° , providing opening angle where the maximum horizontal incidence angle of the sputtered material reaching the sample is $\theta_{TC} = 55.6^\circ$. This is not much more than what the SE collimation provides, but the TC also acts as a shield for scattering of sputtered particles around the chamber (outside the field of view of the target) which is discussed in Section 4.3.

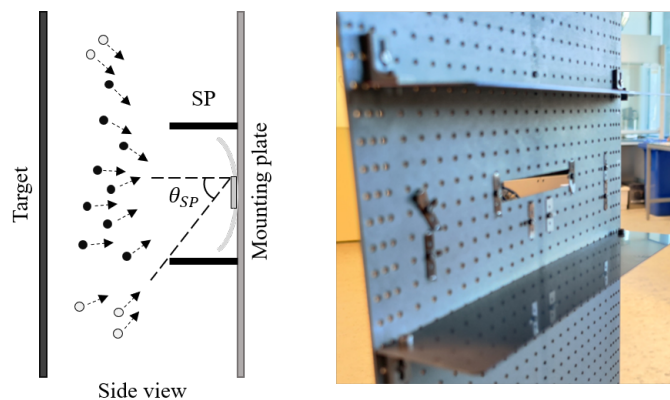


Figure 2: Separator plates (SP) mounted 5 cm above and below the substrate.

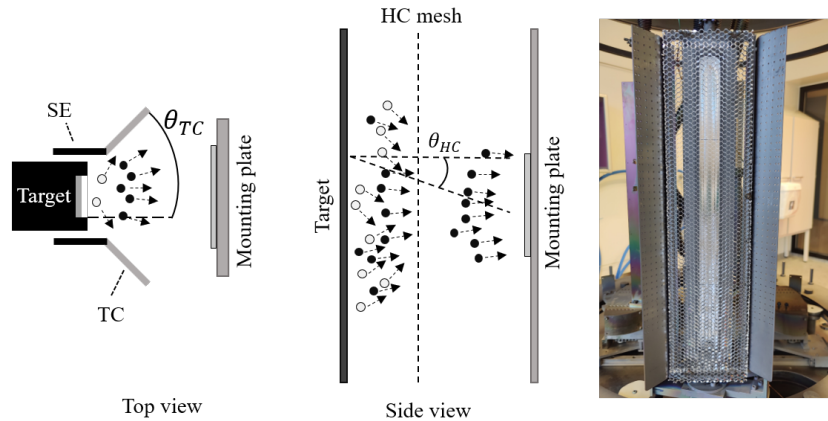


Figure 3: Honey-comb collimator (HC) mounted in front of the target¹⁷, and 45° target collimator (TC) mounted on the side of the target.

The DC magnetron sputtering facility at DTU Space is a high-vacuum chamber²⁰ in which the inert gas argon (Ar), is used during the coating process defined as the sputtering gas. Compounds not native in the target can be formed with reactive sputtering by including a variety of oxides and nitrides etc., to the chamber gas flow. It has been shown that multilayer films consisting of W/B₄C, Co/C, and Ni/C grown in a nitrogen-argon gas mixture that the roughness is reduced compared to non-reactive growth.^{12,21,22} The reactive sputtering process is shown to produce layers that have smaller grain sizes, and superior interface quality, resulting in smoother interfacial roughnesses, and thereby improved X-ray reflecting performances.

The modelling of reactive sputtering is described by Berg's model.^{23–25} A reactive gas such as nitrogen (N₂) will form a compound layer all around the chamber, such as at the target, substrate surface, and the chamber walls etc. During plasma ignition, reactions between the sputtered particles and the reactive gas mainly occurs at the target surface, substrate and walls, and does not occur in the gas phase.²⁵ Though the desired formation of the reaction is mainly located at the substrate, in order for the target to keep a metallic sputtering rate. The compound layer at the target surface will effect the magnetron cathode potential and thereby the deposition rate, chamber pressure and discharge voltage etc.²⁴ At low flow rates of the reactive gas N₂, all of the reactive gas will bind to the sputtered metallic target atoms. A too high N₂ concentration results in a target that is fully covered in the compound, building an insulating layer on the target, defined as target poisoning where the deposition rate falls and the chamber pressure increases. It is therefore important to evaluate different atmosphere concentrations using different gas fractions of Ar/N₂.

The collimators and reactive sputtering will effect the deposition rate (DR), which is a measure of how many nanometers of material are deposited over a length of time. As HEX-P will consist of > 1000 individual mirror segments, it is important that the deposition rate is not reduced too much. Therefore, the measured thickness as a function of ring speed is presented in each section.

3. EXPERIMENTAL PROCEDURE

3.1 Sample preparation

This paper consists of three experimental parts: The collimation of the sputtered material, the study of sputtering gas, and the contamination from a sputtering atmosphere. The purpose of the first two studies is to find an efficient way to suppress the interfacial roughness of the produced NiV/Si multilayer. The purpose of the latter is to evaluate the magnitude of the sputtering atmosphere which may effect the thin film morphology. The samples used in each study are listed in Table 1.

The sputtered thin films presented were produced at the direct-current (DC) magnetron sputtering facility at DTU Space²⁰. We deposited the thin films onto double-side polished silicon substrates, referred to as witness samples, with a crystal orientation (100) and with dimensions 70 mm × 10 mm × 0.775 mm (L × W × H). All witness sample substrates were plasma cleaned prior to the thin film deposition to remove all organic surface contamination, with a power of 400 W for 10 min, in an oxygen (O₂ 200 ml/min)/nitrogen (N₂ 70 ml/min) atmosphere, using a Tepla 300 Semi-Auto Plasma System. Specular reflectometry measurements at 8.048 keV show a decrease in the silicon surface roughness from 0.87 nm to 0.30 nm after plasma cleaning.

Table 1: Samples and associated coating designs in each study. The collimators are shown in Figure 2 and Figure 3.

Study	Coating run	Sample ID	Collimator	NiV gas (Ar%/N ₂ %)	Si gas (Ar%/N ₂ %)
Collimation	1	ds0204-ds0209	SP	100/0	100/0
	2	ds0210-ds0215	SP+TC	100/0	100/0
	3	ds0216-ds0221	SP+TC+HC	100/0	100/0
Sputtering gas	4	ds0225-ds0233	SP+TC	85/15	85/15
	5	ds0234-ds0239	SP+TC	100/0	85/15
	6	ds0240-ds0245	SP+TC	100/0	75/25
Contamination	All	Si-S5	-	-	-

Before thin film deposition, the substrate surfaces are cleaned using a N₂-gun to remove dust and other particulates that could have been deposited onto the surface during the storing of the samples. During the thin film deposition, we applied a power of 350 W, and power density of 1.81 W/cm² to both the NiV and Si target. We preconditioned the NiV and Si target for five minutes in order to remove residual particles that could have adhered to the target surface during the preparation of the chamber for the coating. We performed all coatings with a pressure of 2.8 mTorr, in an atmosphere consisting of a combination of argon (Ar) and nitrogen (N₂). All samples are coated with a periodic 10 bilayer NiV/Si structure, with an aimed bilayer thickness (d) range 4 nm - 20 nm, and an aimed thickness ratio $\Gamma = \frac{z_{NiV}}{d} = 0.5$ where Γ is related to the thickness of the NiV layer z_{NiV} . The samples had a target-to-substrate distance (TSD) of 155 mm, and was rotated around the magnetron during the coating process using calibrated ring rotation speeds.

We initially tried a higher magnetron (cathode) power but resulted in an unstable plasma. A high sputtering power can decrease the interfacial roughness due to less time in the sputtering zone, and increase the deposition rate, though other studies^{9,26} also report that a too high magnetron power can form islands after layer formation which will increase the interfacial roughness.

3.2 X-ray reflectometry characterization

Specular X-ray reflectometry measurements at 8.048 keV were performed with the Finn Christensen X-ray Reflectometer (FCXR²⁰) at DTU Space. The X-ray beam was shaped into a 0.25 × 0.50 mm² (W×H) beam by slits before reaching the sample. The sample to source distance was 1064 mm, and the sample to detector distance was 995 mm, and using a Minipix TPX3 detector.

The measured reflectometry data was fitted using a Python-based software that utilizes the Fresnel equations in combination with a differential evolution algorithm, described in Gellert et al.²⁷. The optical constants for each material are computed using the atomic scattering factors from the Lawrence Livermore National Laboratory (LLNL²⁸). An angular instrumental resolution of 0.007° is specified for the 8.048 keV system. All model structures are composed of a silicon (Si) substrate with a native silicon dioxide (SiO₂) surface layer. The SiO₂ (2.65 g/cm³) thickness was fixed to 2.0 nm (typical value for native grown oxide²⁰) where the roughness was coupled to that of the Si substrate and fixed to 0.3 nm. In the pure Ar coatings, the Si layer density is fixed to that of the nominal density of silicon in the LLNL database (2.33 g/cm³). The NiV layers density are allowed to vary for all measurements, but expect to be near nominal density (8.79 g/cm³), though B. Emprin et al.¹⁴ has reported Ni densities at 7.2 g/cm³ at 8.0 keV. The silicon that is sputtered in a reactive Ar/N₂ atmosphere is varied, since it is reported to chemically change to silicon nitride which has a nominal density a 3.17 g/cm³. All the measured data is initially fitted using only the data with high signal-to-noise ratio, to achieve a good

estimation of the thickness. Thereafter, the data is fitted from $0.25^\circ - 1.4^\circ$, in order to have the same roughness bandwidth for all samples.

3.3 X-ray photoelectron spectroscopy

X-ray photoelectron spectroscopy (XPS) is a technique that measures binding energy of the electrons present in the different structures of the film from where the chemical composition of it can be analyzed. XPS spectra is obtained by illuminating a film with a beam of X-rays, and then measure the number of electrons and their kinetic energies emitted from the film. The measurements were conducted on selected samples using the XPS-Nexsa by ThermoFisher Scientific at DTU Nanolab²⁹. The system operates with a monochromatic micro-focused aluminium (Al) K_α beam (1486.6 eV), with a spot size of $400\text{ }\mu\text{m}^2$, and a takeoff angle of 90° . Both survey scan and high-resolution scans were used. The energy resolution of the survey scans are 1 eV, and the high-resolution scans used 0.1 eV energy resolution with narrow energy band near the bindings energies of selected elements. High-resolution scans were conducted for Ni, V, Si, N, O and Fe. The measured data was processed using the CasaXPS³⁰ software using a Shirley background. The binding energies of different elements were identified using the Thermo Scientific Advantage Data System for XPS, Table of Elements,³¹ the Handbook of X-ray Photoelectron Spectroscopy,³² and the National Institute of Standards and Technology (NIST) XPS database.³³ To investigate the relative atomic concentration within the film (depth-profile), an Ar-ion Gas Cluster source was iteratively used to etch material from the sample using single argon atoms with an monatomic ion energy of 1000 eV with a high current setting.

4. RESULTS AND DISCUSSION

4.1 Sputtering collimators

We show the effect of using three different kinds of sputtering collimators presented in Section 2, by performing specular X-ray reflectometry (XRR) measurements using the 8.048 keV reflectometer (FCXR) at DTU Space on the collimation samples listed in Table 1. Selected samples are analysed using X-ray photoelectron spectroscopy (XPS). XRR and XPS are used to model the thin-film structure, roughness, density, and composition.

Figure 4 shows the XPS survey scan of sample ds0206, at three different depths of etch time (T); at the surface (T = 0 s), in the Si layer (T = 180 s) and in the NiV layer (T = 430 s). The expected elements are present, which includes Ni, V and Si. Iron (Fe) spectral lines are also observed which is not expected. The observed Ar emission lines at binding energies 242.1 eV and 319.1 eV originate from the Ar-ion Gas Cluster source used for the depth-profiling technique. Carbon oxide (CO_x) and hydroxyl oxygen atoms (OH) observed at 285 eV and 533 eV, are only present on the surface and originate from the ambient atmosphere.

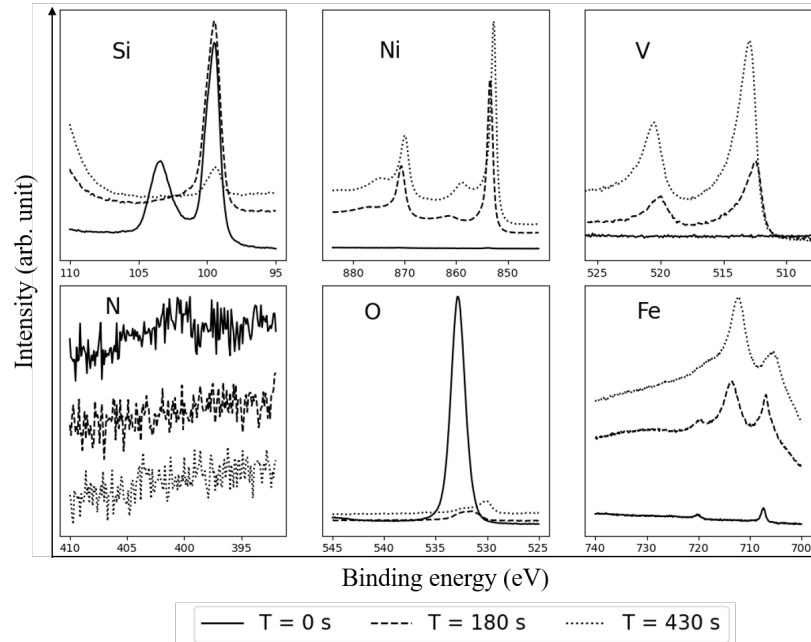


Figure 5: XPS elemental scan of sample ds0206 (SP) at three different depths of etch time (T); at the surface (T = 0 s), in the Si layer (T = 180 s) and in the NiV layer (T = 430 s).

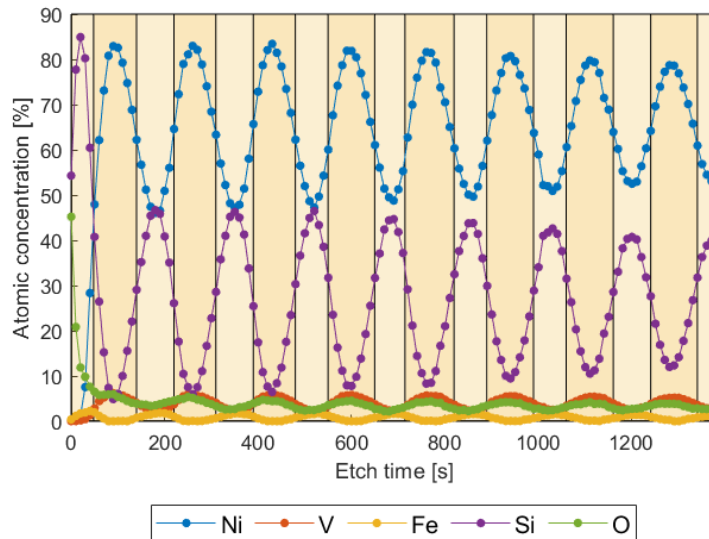


Figure 6: Atomic concentrations derived from XPS depth-profile analyses of the 8 bilayers in sample ds0206 (SP).

The 8.048 keV specular measurements of selected samples including their best-fit models are shown in Figure 7, and the best-fit parameters are listed in Table 2. The measured data was initially fitted using the data with high signal-to-noise ratio in order to achieve a good indication of the thickness. Thereafter, the data was fitted from $0.25^\circ - 1.4^\circ$, in order to have the same roughness bandwidth. We obtained an average NiV density that is 94.4% of nominal density (8.79 g/cm^3). The lower density can be attributed to the measured Fe concentration. Different models were tested which accounted for misalignment, NiVFe compound, variable substrate rough-

nesses, but did not improve the fitted model.

All fitted roughnesses are shown as a function of the thickness in Figure 8. The bilayer roughness is included, as the NiV and Si roughnesses are correlated. It is indicated that using SP with or without the TC, does not reduce the average bilayer roughness. However, the TC can improve the contamination of the sputtering atmosphere in the coating chamber by shielding the back-scattering of the sputtered material which is evaluated in Section 4.3. Figure 9 shows the fitted thickness as a function of the rotating ring speed, for all samples in the collimation study. It is observed that the TC does not effect the NiV or Si deposition rate. It observed that the HC collimation decreases the fitted mean bilayer roughness by a factor of ~ 1.7 , but decreases the mean deposition rate of the Si target by a factor of ~ 2.1 and the NiV target by a factor of ~ 1.85 . This agrees with the results presented by A. Vickery, et al.¹⁷ and D. Girou et al.¹²

Table 2: Fitted model parameters of the 8.048 keV specular reflectivity measurements of selected samples from the collimation study. Figure 7 includes the measured data and fitted model. All measurements are fitted from $0.25^\circ - 1.4^\circ$. Figure 8 includes the fitted thickness as a function of the fitted roughness, for all samples in the collimation study. Figure 9 shows the fitted thickness as a function of the rotating ring speed.

Sample ID	Collimation	Layer	Composition	Thickness (nm)	Density (g/cm ³)	Roughness (nm)
ds0204	SP	Spacer	Si	2.26	2.33 ^c	1.14
		Reflector	NiV	2.39	8.65	1.96
		Substrate oxide	SiO ₂	2.00 ^b	2.65 ^c	0.30 ^{a,b}
		Substrate	Si	-	2.33 ^c	0.30 ^{a,b}
ds0205	SP	Spacer	Si	3.89	2.33 ^c	0.95
		Reflector	NiV	5.06	8.72	1.40
		Substrate oxide	SiO ₂	2.00 ^b	2.65 ^c	0.30 ^{a,b}
		Substrate	Si	-	2.33 ^c	0.30 ^{a,b}
ds0210	SP+TC	Spacer	Si	3.59	2.33 ^c	0.55
		Reflector	NiV	3.86	8.63	2.00
		Substrate oxide	SiO ₂	2.00 ^b	2.65 ^c	0.30 ^{a,b}
		Substrate	Si	-	2.33 ^c	0.30 ^{a,b}
ds0213	SP+TC	Spacer	Si	1.76	2.33 ^c	0.99
		Reflector	NiV	2.47	8.41	2.28
		Substrate oxide	SiO ₂	2.00 ^b	2.65 ^c	0.30 ^{a,b}
		Substrate	Si	-	2.33 ^c	0.30 ^{a,b}
ds0216	SP+TC+HC	Spacer	Si	2.02	2.33 ^c	0.38
		Reflector	NiV	2.33	8.53	1.21
		Substrate oxide	SiO ₂	2.00 ^b	2.65 ^c	0.30 ^{a,b}
		Substrate	Si	-	2.33 ^c	0.30 ^{a,b}
ds0218	SP+TC+HC	Spacer	Si	3.61	2.33 ^c	0.29
		Reflector	NiV	3.64	8.68	0.96
		Substrate oxide	SiO ₂	2.00 ^b	2.65 ^c	0.30 ^{a,b}
		Substrate	Si	-	2.33 ^c	0.30 ^{a,b}

^aCoupled parameters.

^bFixed values based on a priori assumptions (described in text).

^cThe density of silicon and native silicon oxide.

The parameters allowed to vary are presented in bold.

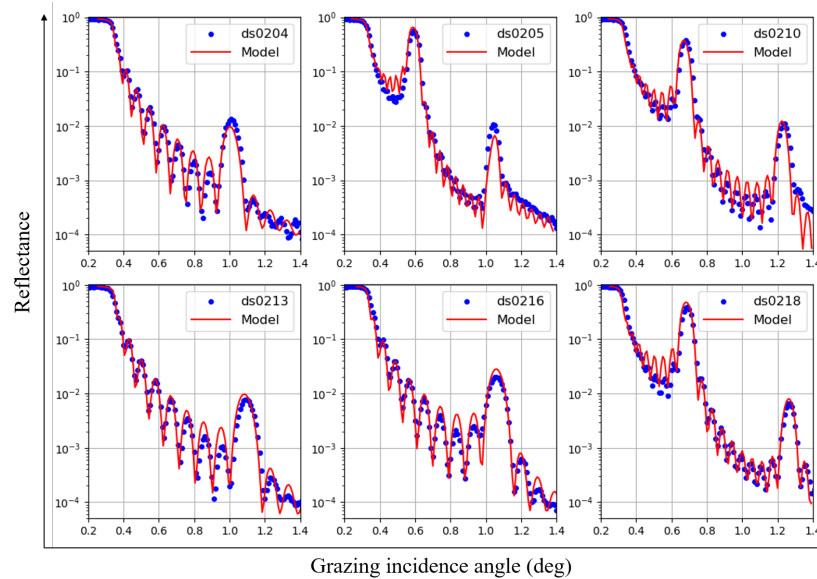


Figure 7: 8.048 keV specular reflectivity measurements of selected samples from the collimation study. The best-fit parameters are listed in Table 2. All measurements are fitted from $0.25^\circ - 1.4^\circ$. Figure 8 includes the fitted thickness as a function of the fitted roughness, for all samples in the collimation study. Figure 9 shows the fitted thickness as a function of the rotating ring speed.

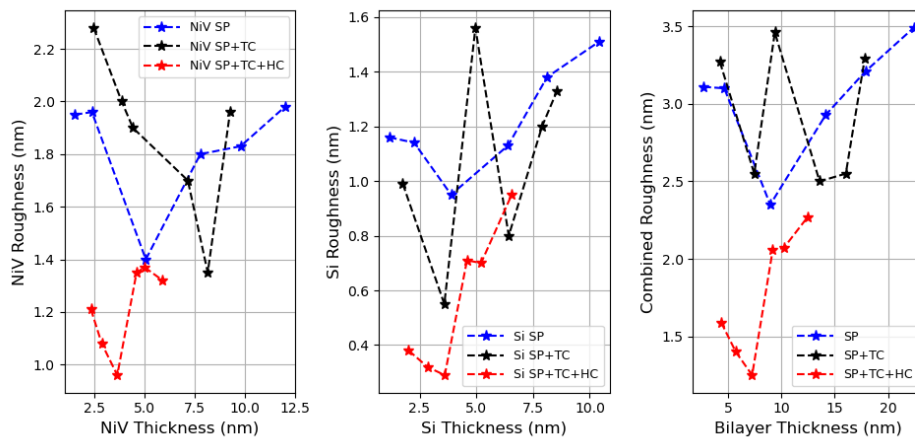


Figure 8: Fitted thickness as a function of the fitted roughness, for all samples in the collimation study.

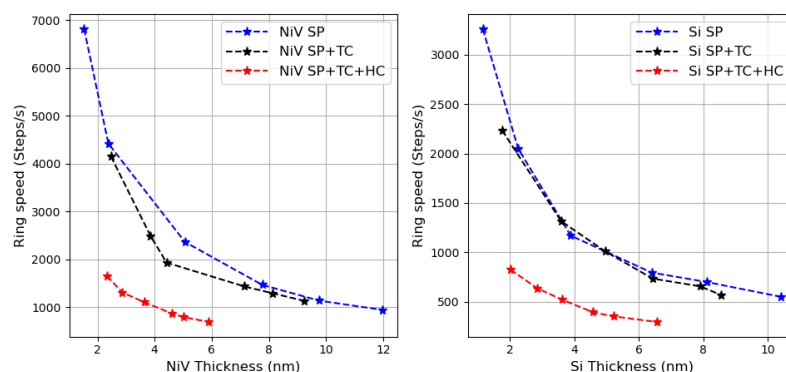


Figure 9: Fitted thickness as a function of the rotating ring speed, for all samples in the collimation study.

4.2 Sputtering gas

Based on the previous results in Sec. 4.1, the reactive sputtering study is performed using the collimation setup which includes the separator plates (SP) and target-collimation (TC), due to that honey-comb (HC) reduced the deposition rate too much. A higher magnetron power was tested, but due to the lack of water cooling pressure in the magnetron, the plasma was unstable which prevented a higher power. The samples and sputtering gas concentrations are listed in Table 1. All samples are characterized using the 8.048 keV XRR at DTU Space, and selected samples are analysed using XPS.

Figure 10 shows the logbook data from the sputtering process of sample ds0229 which includes the power and voltage of the NiV and Si targets, and the pressure during the sputtering process. It is observed that the pressure is not constant, due to Si and NiV reacting with the N_2 . It is observed that the pressure drops more for the Si reactive sputtering, compared to the NiV target sputtering. This indicates that Si is highly reactive with N_2 , compared to NiV.

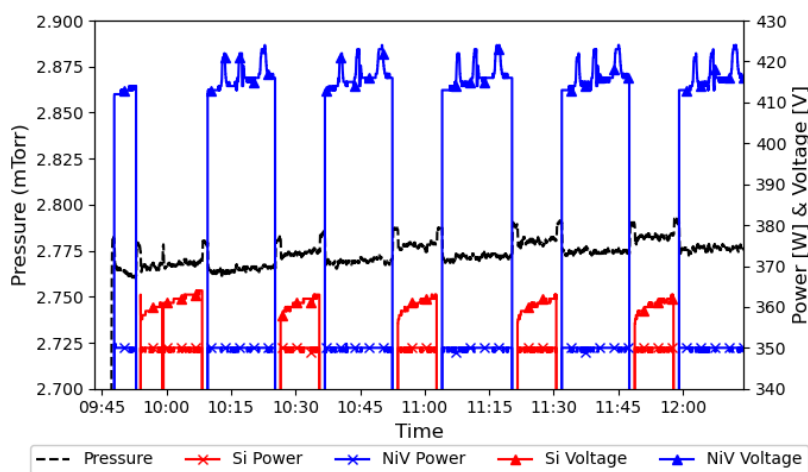


Figure 10: Coating process logbook of the first 5 bilayers for coating run 4 which includes sample ds0229.

Figure 11 shows the XPS survey scan of sample ds0229, at three different depths of etch time (T); at the surface (T = 0 s), in the Si layer (T = 161 s) and in the NiV layer (T = 238 s). The expected elements are

present which includes Ni, V, Si and Fe.

The line at 397.8 eV is a clear indicator that silicon has reacted with nitrogen forming a silicon nitride compound (Si_3N_4)³³ which is not present in the non-reactive. However, there is no evidence of nickel nitridation by the reactive sputtering process. If nickel nitride was present in the film, a clear N 1s peak at 395.8 eV should be visible, and the Ni-Ni bond should be shifted to a higher binding energy at (851.8 eV³⁴), due to the formation of N-Ni bonds.

Figure 12 includes the elemental scans of Ni, V, Si, Fe, N and O. The elemental surface scan of Si shows convoluted peaks of SiO_2 (103.5 eV), Si_3N_4 (101.7 eV) and metallic Si (99.4 eV).³¹ Through the depth profile, the elemental scan of Si shows that a large amount of the Si 2p at 99.4 eV, is shifted to 101.7 eV due to the formation of silicon nitride.³⁵

The elemental scans of Ni, V, O, and Fe indicate no shift in peaks compared to the non-reactive sample in Section 4.1, though a convoluted peak at 514 eV due to vanadium nitrite can explain the reactive process observed in the logbook during the NiV sputtering. The survey scan of nitrogen clearly shows the Si_3N_4 peak at 397.8 eV, and the 396.8 eV peak can be attributed vanadium nitrite. Figure 13 shows the atomic concentrations derived from depth-profile analyses of the 4 bilayers in sample ds0229. Here it is observed that N is largely present in the Si layers.

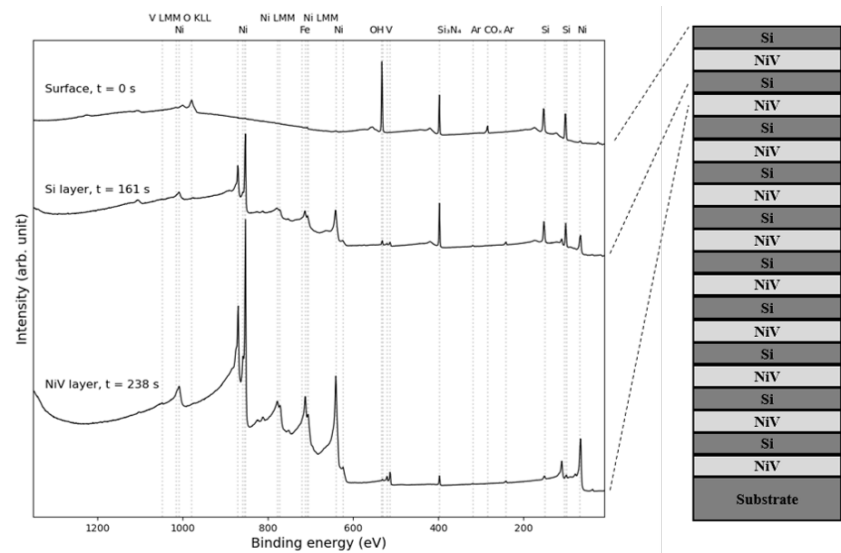


Figure 11: XPS survey scan of sample ds0229 (SP+TC), reactively sputtered on both targets with a 85% Ar / 15% N_2 reactive sputtering concentration, at three different depths of etch time (T); at the surface (T = 0 s), in the Si layer (T = 161 s) and in the NiV layer (T = 238 s).

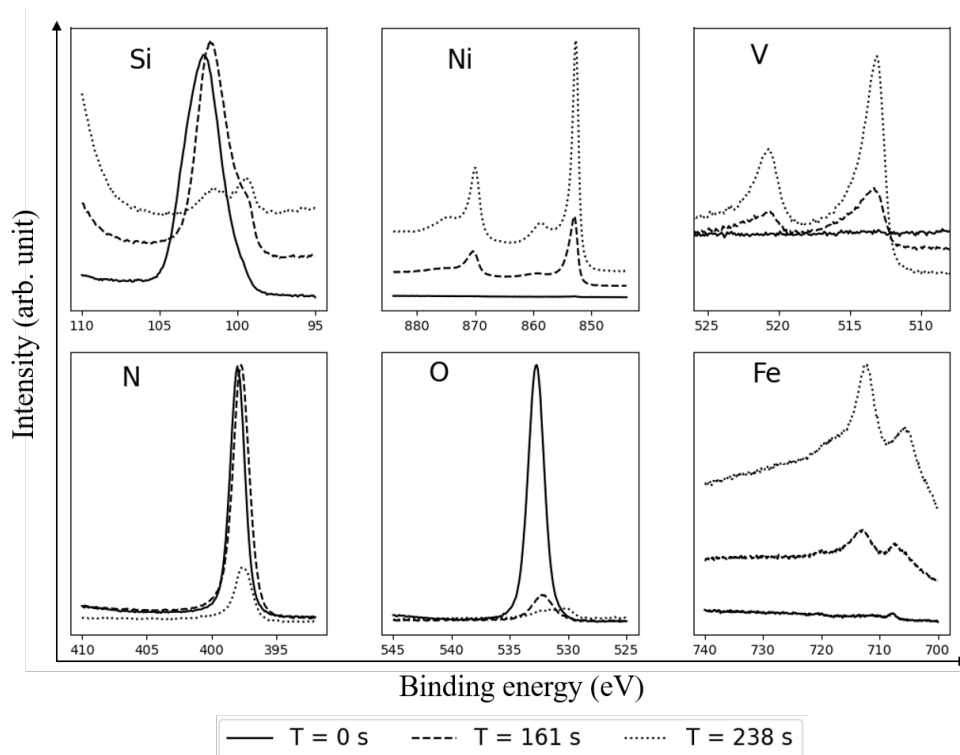


Figure 12: XPS elemental scan of sample ds0229 (SP+TC), reactively sputtered on both targets with a 85% Ar / 15% N₂ gas concentration, at three different depths of etch time (T); at the surface (T = 0 s), in the Si layer (T = 161 s) and in the NiV layer (T = 238 s).

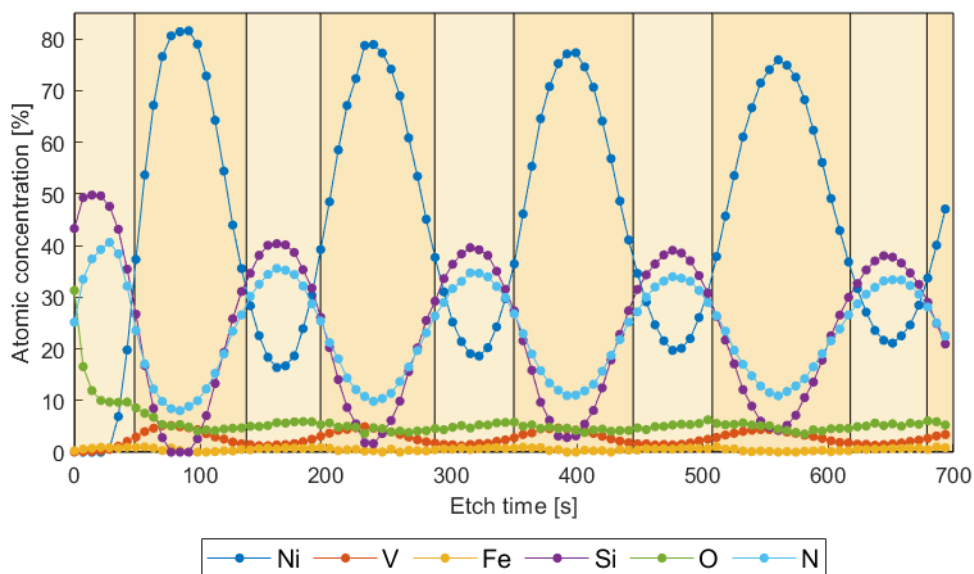


Figure 13: Atomic concentrations derived from XPS depth-profile analyses of the 4 bilayers in sample ds0229 (SP+TC), reactively sputtered on both targets with a 85% Ar / 15% N₂ gas concentration.

The 8.048 keV specular measurements of selected samples including their best-fit models are shown in Figure 14, and the best-fit parameters are listed in Table 3. Similar to Section 4.1, the measured data was initially fitted using the data with high signal-to-noise ratio, to achieve a good indication of the thickness. Thereafter, the data was fitted from $0.25^\circ - 1.4^\circ$, in order to have the same roughness bandwidth for all samples. The samples where NiV was coated reactively (Coating 4) showed smoothened Kiessig fringes that presented modeling challenges, as shown for samples ds0231 and ds0233 in Figure 14. This indicates that these samples have a higher roughness than what is obtained from the XRR fits.

The reactive sputtering process will affect the chemical composition of the sputtered material, and therefore the Si density is not a fixed parameter for these measurements. It is expected that the density of the silicon layers approximate Si_3N_4 at 3.17 g/cm^3 . For the Si reactive sputtering samples which included a sputtering gas concentration of 85% Ar/15% N_2 , we obtained a mean density of 2.80 g/cm^3 , and for samples coated with a 75% Ar/25% N_2 concentration the mean density was 2.95 g/cm^3 . This indicates that a higher concentration of N_2 produces a more pure Si_3N_4 compound. We obtained an average NiV density that is 86% of nominal density for the reactively sputtered NiV thin films, and 93% of nominal density for coating run 5 and 6 which is similar to the results presented in Section 4.1.

All fitted roughnesses are shown as a function of the thickness in Figure 15. The bilayer roughness is included, as the NiV and Si roughness can be correlated. It is indicated from the combined bilayer roughness in coating run 4 that reactively sputtering NiV induces a high roughness. It is indicated from coating run 5 that reactively coating Si using a sputtering gas concentration of 85% Ar/15% N_2 does improve the interfacial roughness, however, coating run 6 shows that a too large concentration of N_2 will negatively effect the roughness. These results agree with a visual analysis of the 8.048 keV XRR spectrums, comparing the reflectivity slope and the depth of the kiessig fringes.

Figure 16 shows the fitted thickness as a function of the rotating ring speed for all samples in the sputtering gas study. Is observed that reactively sputtered NiV will reduce the deposition rate which shows that NiV does react with the N_2 -gas, confirmed by the drop in pressure observed in the the coating process logbook. Reactive sputtered Si does not affect the deposition rate in the experiments conducted, indicating that there was no target poisoning

Table 3: Fitted model parameters of the 8.048 keV specular reflectivity measurements of selected samples from the sputtering gas study. Figure 14 includes the measured data and fitted model. All measurements are fitted from $0.25^\circ - 1.4^\circ$. Figure 15 includes the fitted thickness as a function of the fitted roughness, for all samples in the study. Figure 16 shows the fitted thickness as a function of the rotating ring speed.

Sample ID	Coating run	Layer	Composition	Thickness (nm)	Density (g/cm ³)	Roughness (nm)
ds0231	4	Spacer	Si	1.82	3.13	1.4
		Reflector	NiV	1.89	7.22	0.8
		Substrate oxide	SiO ₂	2.00 ^b	2.65 ^c	0.30 ^{a,b}
		Substrate	Si	-	2.33 ^c	0.30 ^{a,b}
ds0233	4	Spacer	Si	3.69	3.27	1.02
		Reflector	NiV	4.02	7.58	0.97
		Substrate oxide	SiO ₂	2.00 ^b	2.65 ^c	0.30 ^{a,b}
		Substrate	Si	-	2.33 ^c	0.30 ^{a,b}
ds0237	5	Spacer	Si	1.80	2.99	0.62
		Reflector	NiV	2.38	7.84	0.52
		Substrate oxide	SiO ₂	2.00 ^b	2.65 ^c	0.30 ^{a,b}
		Substrate	Si	-	2.33 ^c	0.30 ^{a,b}
ds0239	5	Spacer	Si	3.55	3.18	1.00
		Reflector	NiV	4.59	8.49	0.88
		Substrate oxide	SiO ₂	2.00 ^b	2.65 ^c	0.30 ^{a,b}
		Substrate	Si	-	2.33 ^c	0.30 ^{a,b}
ds0243	6	Spacer	Si	2.42	2.96	0.83
		Reflector	NiV	2.38	8.09	0.92
		Substrate oxide	SiO ₂	2.00 ^b	2.65 ^c	0.30 ^{a,b}
		Substrate	Si	-	2.33 ^c	0.30 ^{a,b}
ds0245	6	Spacer	Si	4.55	2.96	1.05
		Reflector	NiV	4.12	8.11	0.86
		Substrate oxide	SiO ₂	2.00 ^b	2.65 ^c	0.30 ^{a,b}
		Substrate	Si	-	2.33 ^c	0.30 ^{a,b}

^aCoupled parameters.

^bFixed values based on a priori assumptions (described in text).

^cThe density of silicon and native silicon oxide.

The parameters allowed to vary are presented in bold.

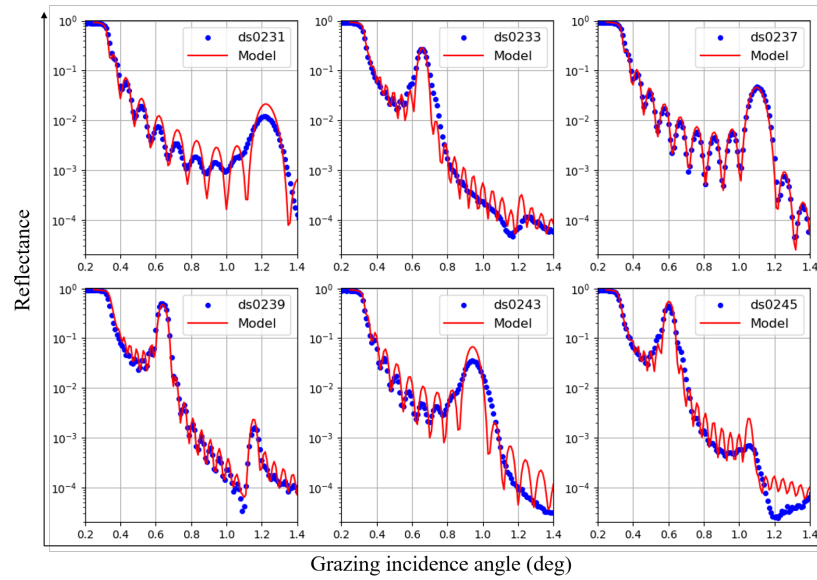


Figure 14: 8.048 keV specular reflectivity measurements of selected samples from the sputtering gas study. The best-fit parameters are listed in Table 3. All measurements are fitted from $0.25^\circ - 1.4^\circ$. Figure 15 includes the fitted thickness as a function of the fitted roughness, for all samples in the gas study. Figure 16 shows the fitted thickness as a function of the rotating ring speed.

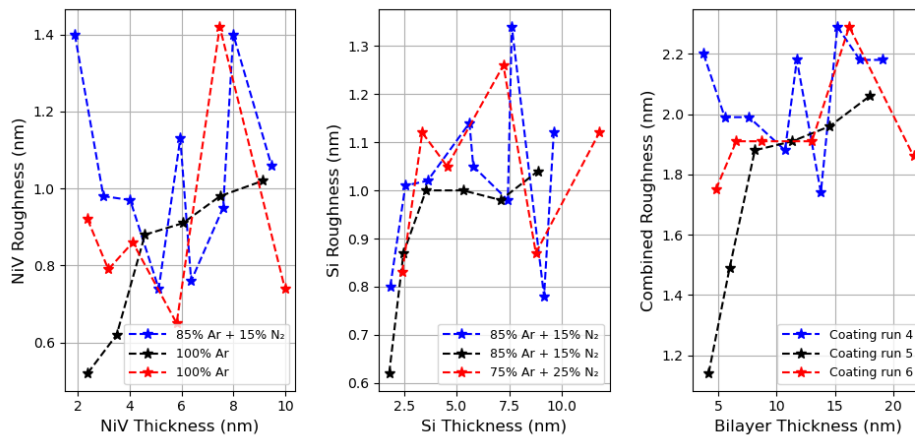


Figure 15: Fitted thickness as a function of the fitted roughness, for all samples in the sputtering gas study.

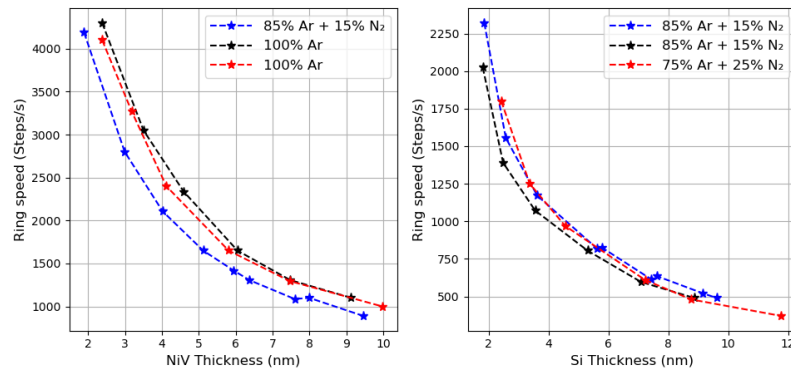


Figure 16: Fitted thickness as a function of the rotating ring speed, for all samples in the sputtering gas study.

4.3 Chamber sputtering contamination

The purpose of this study was to evaluate the uniformity of the sputtering atmosphere in the coating chamber. In previous studies, it has been assumed that the deposition follows a straight line drawn perpendicular to the center of the target, with a solid angle of sputtered particles that can be controlled by using the mentioned collimations.¹⁶ Though visual remnants of sputtering has been observed in previous studies that are outside the field of view of the targets which can contribute to the interfacial roughnesses. In order to evaluate the chamber sputtering atmosphere, five witness samples have been mounted around the chamber for the entire duration of this study where the sample positions and chamber is illustrated in Figure 17, including an image of the five samples.

A visual inspection of the samples indicate that there is no coating on sample S1 and S2 which are respectively mounted in the turbo pump outflow hatch and mounted at the center of the chamber. Sample S3, S4 and S5 show clear indication of thin film deposition which are mounted on the unused Magnetron 2, with a sample mounted pointing towards the NiV target, on top of the magnetron, and towards the Si target, respectively. It is observed that sample S4 and S5 include a blue-tinted color which is due to a thin silicon oxide layer. The fact that there is deposited visual Si and NiV from the sputtering process that is outside the sputtering field of view, provides evidence that the sputtered atoms undergo collisions with each other and the working gas or chamber walls.

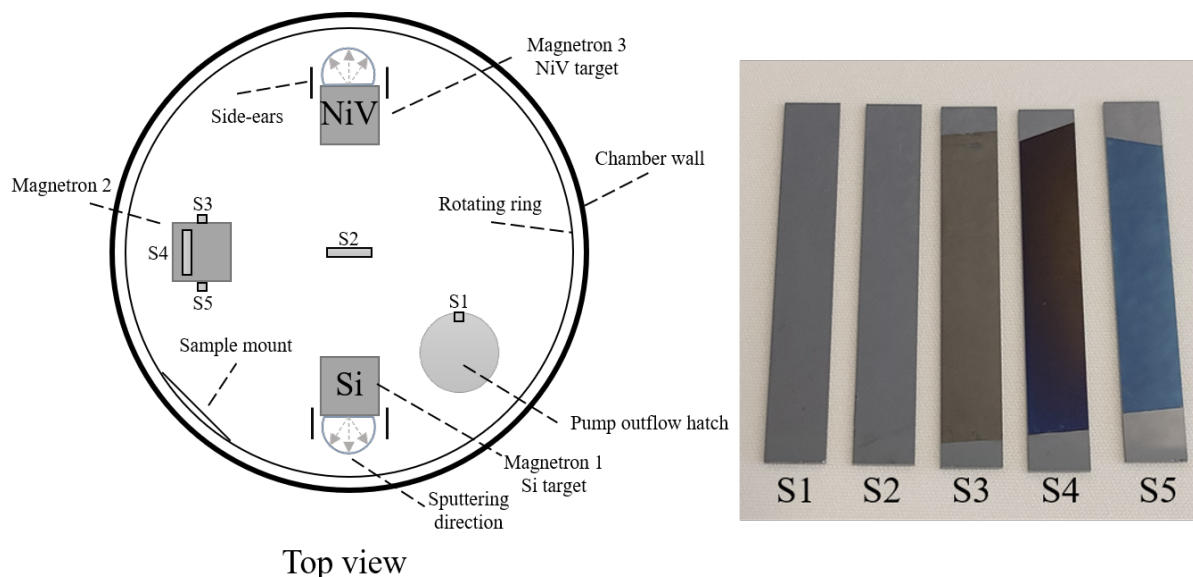


Figure 17: Illustration of the DC magnetron coating chamber at DTU Space^{13, 20, 36} and the sample positions of contamination samples S1-S5, including an image of the samples. As illustrated, samples S1, S3 and S5 are mounted vertically, and samples S2 and S4 are mounted horizontally.

XPS survey scans have been conducted on each of the contamination samples, and are shown in Figure 18. The survey scans of sample S1 and S2 are of the sample subsurface after 4.0 seconds Ar-ion etching which removes the hydrocarbon-rich surface, and does not change the resolution or intensity of the other peaks. Sample S3-S5 are of the sample interior after 8.0 seconds Ar-ion etching. Figure 18 includes identification of the elements that are responsible for the individual emission lines.

The survey scans show that all five samples S1-S5 include elemental concentrations from the sputtering targets. This provides evidence that there is a non-uniform atmosphere of the sputtered particles during the sputtering process which could have an affect on the morphology and roughness of the thin films produced in the DC magnetron sputtering chamber at DTU Space.

Samples S1 and S2 do not have a visual thick layer, so the measured concentrations can also be attributed to cross contamination from opening of chamber and sample transfer. However it is evident that there is a non-uniform atmosphere of the sputtered particles during the sputtering process. This could be minimized by using more collimators and sputtering shields.

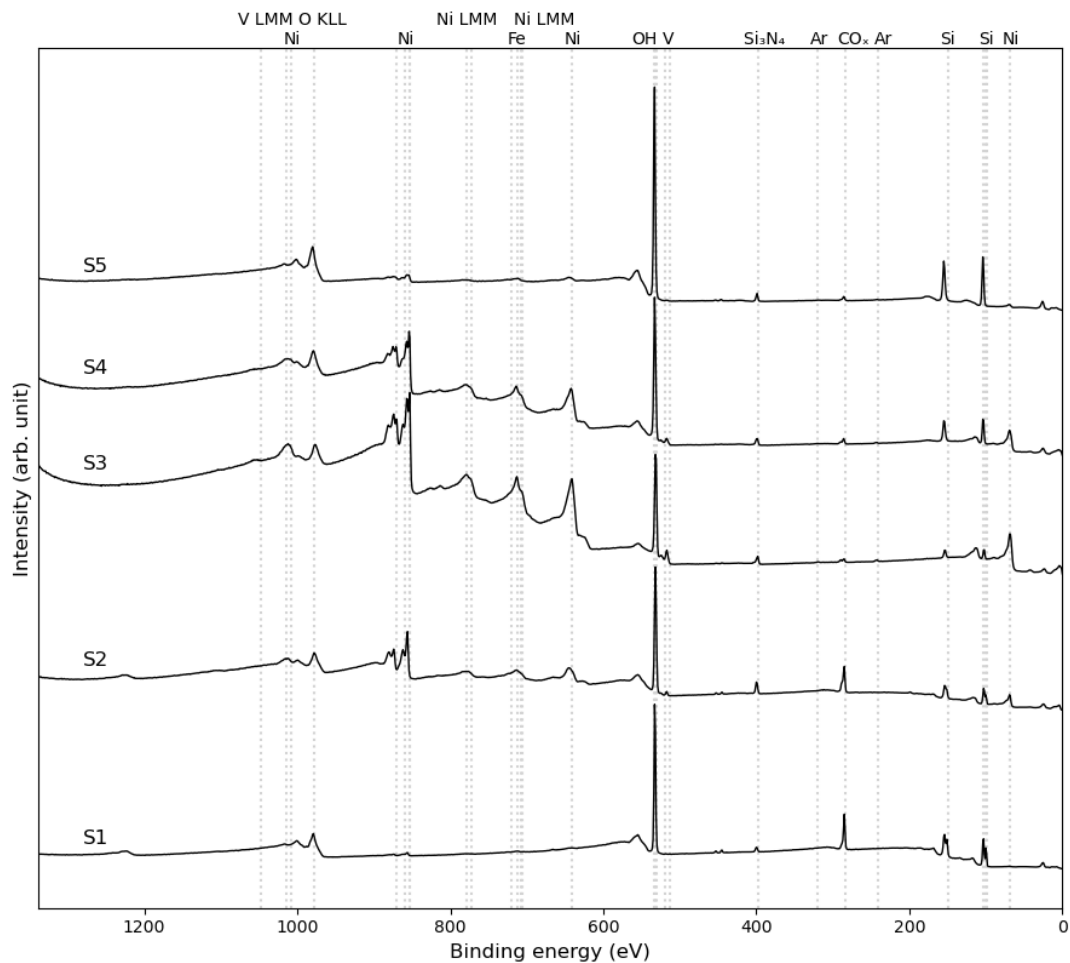


Figure 18: XPS survey scan of contamination samples S1-S5. Their individual positions in the coating chamber is illustrated in Figure 17.

5. FUTURE WORK

There is still a lot of work to be done on the NiV material in order to be characterized as possible flight quality for HEX-P. For a thorough and complete study of Ni as the reflecting material for HEX-P, we introduce a possible method of progress. The first step should be to characterise Ni and NiV as single layers and obtain the roughness as a function of thickness, and use methods to minimize grain size and roughness, such as:

- Substrate bias voltage. Applying a bias voltage on the substrate causes the ions that are created between the bias layer and the substrate, to be accelerated towards the target which can effect the microstructure and properties of the sputtered thin films.
- Substrate heating. Sputtering on heated substrates can provide the sputtered adatoms with enough kinetic surface energy to rearrange themselves to construct a more dense and compact crystalline structure which can impact the microstructure and properties of the sputtered thin films.
- Target collimators. Test new collimation types which will minimize the incidence of the sputtered material and shield for back-sputtering, to minimize the interfacial contamination and roughness, and to ensure uniform layer thickness.

- Sputtering gas concentrations. Investigate different reactive gasses and gas concentrations to lower the interfacial roughness.
- Cathode power. A high sputtering power can decrease the interfacial roughness due to less time in the sputtering zone and increase the deposition rate, though a too high power can form islands after layer formation.
- Double target pass. In case the deposition rate is low, it should be investigated if using two magnetrons to build a layer effects the thin film roughness.

Thereafter, these steps should be repeated for a NiV/Si multilayer consisting of 10 bilayers, and then 150 bilayer power law coating. It would be interesting to obtain results of NiV multilayers produced from different deposition facilities and methods. In previous work, a thin Si layer was mistakenly deposited on the substrate as a bottom layer in a NiV/Si multilayer which reduced the interfacial roughness. Multiple flow-meters have since this study been installed in the DTU Space coating facility in order to monitor the pressure of the water cooling system. Furthermore, new and larger magnetrons are being installed and tested, with new collimators and target shields.

6. SUMMARY

As part of the thin film coating development for the High Energy X-ray Probe (HEX-P) which is a NASA probe-class mission concept, we have investigated two methods to reduce the interfacial roughness in periodic NiV/Si multilayers coatings. We have evaluated thin film coatings sputtered using different types of sputtering collimators and different reactive sputtering gas concentrations, deposited on smooth Si substrates using DC magnetron sputtering at DTU Space. The multilayers are characterized using X-ray reflectometry and X-ray photoelectron spectroscopy which is used to model the thin-film structure, roughness, density, and composition.

Collimation of the sputtered particles plays an important role in the production of thin film coatings with low roughness, and in this paper we evaluate the separator plate (SP) collimation and honey-comb (HC) collimation, and a new target collimator (TC). It is shown that using SP with or without the TC, does not reduce the average bilayer roughness in the the NiV/Si multilayer. However, the HC collimation decreases the mean bilayer roughness by a factor of ~ 1.6 , but decreases the deposition rate of both targets by a factor of ~ 2.0 .

The reactive sputtering process with Ar/N₂ is known to produce layers with superior interface quality, resulting in smoother interfacial roughnesses, and thereby improved X-ray reflecting performances. We have evaluated the NiV/Si multilayers coated with different gas fractions of Ar/N₂. We have shown that reactively coating Si using a sputtering gas concentration of 85% Ar/15% N₂ does improve the interfacial roughness, however a too high concentration of N₂ will have a negative impact on the roughness as the Si will chemically react with N₂ and form a pure Si₃N₄ layer. We show that reactively sputtering NiV with N₂ increases the interfacial roughness.

For the entire duration of this study five silicon samples have been mounted around the sputtering chamber in order to evaluate the uniformity of the sputtering atmosphere inside the coating chamber. The samples showed that NiV and Si was deposited outside the field of view of the targets which can contribute to the interfacial roughnesses of the thin films produced in the DC magnetron sputtering chamber at DTU Space.

REFERENCES

- [1] Furuzawa, A., Ogasaka, Y., Kunieda, H., Miyazawa, T., Sakai, M., Kinoshita, Y., Makinae, Y., Sasaya, S., Kanou, Y., Niki, D., Ohgi, T., Oishi, N., Yamane, K., Yamane, N., Ishida, Y., Haba, Y., Tawara, Y., Yamashita, K., Ishida, M., Maeda, Y., Mori, H., Tamura, K., Awaki, H., and Okajima, T., "The current status of ASTRO-H/HXT development facility," in [*Optics for EUV, X-Ray, and Gamma-Ray Astronomy IV*], O'Dell, S. L. and Pareschi, G., eds., **7437**, 79 – 86, International Society for Optics and Photonics, SPIE (2009).

- [2] Mori, H., Miyazawa, T., Awaki, H., Matsumoto, H., Babazaki, Y., Bandai, A., Demoto, T., Furuzawa, A., Haba, Y., Hayashi, T., Iizuka, R., Ishibashi, K., Ishida, M., Ishida, N., Itoh, M., Iwase, T., Kato, H., Kobayashi, H., Kosaka, T., Kunieda, H., Kurashima, S., Kurihara, D., Kuroda, Y., Maeda, Y., Meshino, Y., Mitsuishi, I., Miyata, Y., Nagano, H., Namba, Y., Ogasaka, Y., Ogi, K., Okajima, T., Saji, S., Shimasaki, F., Sato, T., Sato, T., Shima, N., Sugita, S., Suzuki, Y., Tachibana, K., Tachibana, S., Takizawa, S., Tamura, K., Tawara, Y., Tomikawa, K., Torii, T., Uesugi, K., Yamashita, K., and Yamauchi, S., “On-ground calibration of the Hitomi Hard X-ray Telescopes,” *Journal of Astronomical Telescopes, Instruments, and Systems* **4**(1), 011210 (2018).
- [3] Koglin, J. E., An, H., Blaedel, K. L., Brejnholt, N. F., Christensen, F. E., Craig, W. W., Decker, T. A., Hailey, C. J., Hale, L. C., Harrison, F. A., Jensen, C. P., Madsen, K. K., Mori, K., Pivovarov, M. J., Tajiri, G., and Zhang, W. W., “NuSTAR hard x-ray optics design and performance,” in [*Optics for EUV, X-Ray, and Gamma-Ray Astronomy IV*], O’Dell, S. L. and Pareschi, G., eds., **7437**, 107 – 114, International Society for Optics and Photonics, SPIE (2009).
- [4] Christensen, F. E., Jakobsen, A. C., Brejnholt, N. F., Madsen, K. K., Hornstrup, A., Westergaard, N. J., Momberg, J., Koglin, J., Fabricant, A. M., Stern, M., Craig, W. W., Pivovarov, M. J., and Windt, D., “Coatings for the NuSTAR mission,” in [*Optics for EUV, X-Ray, and Gamma-Ray Astronomy V*], O’Dell, S. L. and Pareschi, G., eds., **8147**, 298 – 316, International Society for Optics and Photonics, SPIE (2011).
- [5] Brejnholt, N., Christensen, F., Westergaard, N., Hailey, C., Koglin, J., and Craig, W., “Nustar on-ground calibration ii: Effective area,” *Proceedings of SPIE, the International Society for Optical Engineering*, SPIE - International Society for Optical Engineering (2012). SPIE Astronomical Telescopes + Instrumentation 2012, conference 8443, paper 70.; SPIE Astronomical Telescopes + Instrumentation 2012 ; Conference date: 01-07-2012 Through 06-07-2012.
- [6] Probst, A.-C., Begou, T., Döhring, T., Zeising, S., Stollenwerk, M., Stadtmüller, J., Emmerich, F., and Lumeau, J., “Coating stress analysis and compensation for iridium-based x-ray mirrors,” *Appl. Opt.* **57**, 8775–8779 (Oct 2018).
- [7] “The high energy x-ray probe.” hexp.org. Accessed: 2022-11-14.
- [8] Tiwari, S. K., Rao, A. U., Chawla, V., Dubey, P., Saxena, V., Chawla, A. K., and Avasthi, D. K., “Synthesis and characterization of sputter-deposited ni-rich ni₃al hard coatings,” *Journal of Alloys and Compounds* **926**, 166802 (2022).
- [9] Ginley, T., “Optimizing sputtering parameters to minimize roughness in permalloy thin films.” https://www.ncnr.nist.gov/programs/CHRS/pdfs/SURF/2011_Ginley.pdf. [Online; accessed 28-April-2023].
- [10] Chaparro, W. A. A. and Lopez, E. V., “Electrodeposition of nickel plates on copper substrates using PC y PRC,” (2007).
- [11] Gurgew, D., “Development of ni-based multilayer coatings for extended broadband x-ray imaging.” Poster at SPIE, Space Telescopes and Instrumentation 2022. Ultraviolet to Gamma Ray.
- [12] Girou, D. A., Massahi, S., Sleire, E. K., Jakobsen, A. C., and Christensen, F. E., “Development of Ni-based multilayers for future focusing soft gamma ray telescopes,” in [*Society of Photo-Optical Instrumentation Engineers (SPIE) Conference Series*], *Society of Photo-Optical Instrumentation Engineers (SPIE) Conference Series* **9603**, 96031D (Sept. 2015).
- [13] Massahi, S., Ferreira, D., Christensen, F., Gellert, N., Svendsen, S., Henriksen, P., Jegers, A. S., Collon, M., Landgraf, B., Girou, D., Thete, A., Shortt, B., Ferreira, I., Bavdaz, M., Schönberger, W., and Langer, A., “The effect of deposition process parameters on thin film coatings for the Athena X-ray optics,” in [*Optics for EUV, X-Ray, and Gamma-Ray Astronomy X*], O’Dell, S. L., Gaskin, J. A., and Pareschi, G., eds., **11822**, 118220B, International Society for Optics and Photonics, SPIE (2021).
- [14] Emprin, B., Troussel, P., Soullié, G., Stemmler, P., Mercère, P., Meltchakov, E., Jérôme, A., and Delmotte, F., “X-ray broadband ni/sic multilayers: improvement with w barrier layers,” *Opt. Express* **22**, 25853–25865 (Oct 2014).
- [15] Paul, A., Lim, J., Choi, K., and Lee, C., “Effects of deposition parameters on the properties of chromium carbide coatings deposited onto steel by sputtering,” *Materials Science and Engineering: A* **332**(1), 123–128 (2002).

- [16] Gellert, N. C., Massahi, S., Salmaso, B., Spiga, D., Ferreira, D., Vecchi, G., Ferreira, I., Bavdaz, M., Basso, S., Svendsen, S., Jegers, A. S., and Christensen, F. E., “Performance of the thin film coating on the long and collimating BEaTriX parabolic mirror,” *Journal of Astronomical Telescopes, Instruments, and Systems* **9**(2), 024004 (2023).
- [17] Vickery, A., Cooper-Jensen, C., Christensen, F., Steenstrup, M., and Schønfeldt, T., “Collimated magnetron sputter deposition for mirror coatings,” *X-Ray Optics and Instrumentation*, **9** (2008).
- [18] Dalla Torre, J., Gilmer, G. H., Windt, D. L., Kalyanaraman, R., Baumann, F. H., O’Sullivan, P. L., Sapjeta, J., Diaz de la Rubia, T., and Djafari Rouhani, M., “Microstructure of thin tantalum films sputtered onto inclined substrates: Experiments and atomistic simulations,” *Journal of Applied Physics* **94**(1), 263–271 (2003).
- [19] Mucha, J., Szytuła, A., and Kwiatkowska, C., “Magnetic properties of nickel-vanadium alloys,” *Journal of Magnetism and Magnetic Materials* **42**(1), 53–58 (1984).
- [20] Massahi, S., *Industrialization of the mirror plate coatings for the ATHENA mission*, PhD thesis (2019).
- [21] Bellotti, J. A. and Windt, D. L., “Depth-graded Co/C multilayers prepared by reactive sputtering,” in [*Optics for EUV, X-Ray, and Gamma-Ray Astronomy IV*], O’Dell, S. L. and Pareschi, G., eds., **7437**, 743715, International Society for Optics and Photonics, SPIE (2009).
- [22] Windt, D., “Reduction of stress and roughness by reactive sputtering in w/b4c x-ray multilayer films - art. no. 66880r,” *Proceedings of SPIE - The International Society for Optical Engineering* **6688** (09 2007).
- [23] Adachi, H., Hata, T., and Wasa, K., “5 - basic process of sputtering deposition,” in [*Handbook of Sputtering Technology (Second Edition)*], Wasa, K., Kanno, I., and Kotera, H., eds., 295–359, William Andrew Publishing, Oxford, second edition ed. (2012).
- [24] Dane, A. E., “Reactive dc magnetron sputtering of ultrathin superconducting niobium nitride films,” Master of Science in Electrical Engineering, Massachusetts Institute of Technology, 2015.
- [25] Bandorf, R., “Application of reactive sputtering,” SVC Web-Tutorial 338, Fraunhofer IST, 2020.
- [26] Mustafa, M., Majeed, U., and Iqbal, Y., “Effect on silicon nitride thin films properties at various powers of rf magnetron sputtering,” *International Journal of Engineering Technology* **7**, 39–41 (08 2018).
- [27] Gellert, N. C., Massahi, S., Ferreira, D. D. M., Christensen, F. E., Svendsen, S., Jegers, A. S., and Madsen, K. K., “Optimization of multilayer coatings for future high-energy focusing telescopes,” in [*Space Telescopes and Instrumentation 2022: Ultraviolet to Gamma Ray*], den Herder, J.-W. A., Nikzad, S., and Nakazawa, K., eds., **12181**, 121814K, International Society for Optics and Photonics, SPIE (2022).
- [28] Red Cullen, L. E. A. D. L. <https://www-nds.iaea.org/epd197/za1to100.htm>. [Retrieved July 5th 2021].
- [29] “Dtu nanolab.” www.nanolab.dtu.dk/english. [Online; accessed 21-May-2023].
- [30] Fairley, N., Fernandez, V., Richard-Plouet, M., Guillot-Deudon, C., Walton, J., Smith, E., Flahaut, D., Greiner, M., Biesinger, M., Tougaard, S., Morgan, D., and Baltrusaitis, J., “Systematic and collaborative approach to problem solving using x-ray photoelectron spectroscopy,” *Applied Surface Science Advances* **5** (Sept. 2021). Publisher Copyright: © 2021 The Authors.
- [31] “Thermo scientific advantage data system for xps, table of elements.” <https://www.thermofisher.com/dk/en/home/materials-science/learning-center/periodic-table.html>. [Retrieved 2023].
- [32] Moulder, J. and Chastain, J., [*Handbook of X-ray Photoelectron Spectroscopy: A Reference Book of Standard Spectra for Identification and Interpretation of XPS Data*], Physical Electronics Division, Perkin-Elmer Corporation (1992).
- [33] “National institute of standards and technology (nist) x-ray photoelectron spectroscopy database.” <https://srdata.nist.gov/xps/EnergyTypeValSrch.aspx>. [Retrieved 2023].
- [34] Kang, J., Park, M.-A., Jae-Yup, K., Park, S., Chung, D., Yu, S.-H., Kim, J., Park, J., Choi, J.-W., Lee, K. J., Jeong, J., Ko, M., Ahn, K.-S., and Sung, Y.-E., “Reactively sputtered nickel nitride as electrocatalytic counter electrode for dye- and quantum dot-sensitized solar cells,” *Scientific reports* **5**, 10450 (05 2015).

- [35] Dieguez, L., Caballero, D., Calderer, J., Moreno, M., Martinez, E., and Samitier, J., “Optical gratings coated with thin Si_3N_4 layer for efficient immunosensing by optical waveguide lightmode spectroscopy,” *Biosensors* **2**, 114–126 (12 2012).
- [36] Brejnholt, N., “Nustar calibration facility and multilayer reference database: Optic response model comparison to nustar on-ground calibration data,” PhD thesis, Technical University of Denmark, 2012.